

**PHYSIOLOGIC CHARACTERIZATION OF HUMAN OVARIAN CANCER CELLS IN  
A RAT MODEL OF INTRAPERITONEAL ANTINEOPLASTIC THERAPY**

Michael F. Flessner, Jaehwa Choi, Zhi He, Kimberly Credit  
University of Mississippi Medical Center  
Jackson, Mississippi

Running Title: Rat Model of IP Therapy

Correspondence to:

Michael F. Flessner, MD, PhD  
Division of Nephrology, Department of Medicine  
University of Mississippi Medical Center  
2500 North State Street  
Jackson, MS 39216-4505

Ph: 601-984-5670

FAX: 601-984-5765

Email: [mflessner@medicine.umsmed.edu](mailto:mflessner@medicine.umsmed.edu)

## ABSTRACT

Destruction of cancer cells by therapies directed against new molecular targets requires their effective delivery to the tumor. To study diffusion and convection of intraperitoneal (ip) therapy to ip tumors, we established a new athymic rat (RNU) model with ovarian tumor cells (SKOV3 and OVCAR3) implanted in the abdominal wall. The model simulates metastatic tumor and facilitates the measurement of physiological parameters that govern transport forces. CD-31 immunohistochemistry revealed unique patterns of angiogenesis, with a tissue-averaged vascular volume of  $\sim 0.01$  ml/g for each tumor. The extracellular volume ( $0.54 \pm 0.11$  ml/g,  $n=5$ , SKOV3;  $0.61 \pm 0.03$ ,  $n=5$ , OVCAR3) was over twice that of the adjacent normal muscle ( $0.22 \pm 0.06$  ml/g,  $n=5$ ). Iv-injected antibody tumor clearance was two to three times that of muscle. Interstitial pressures were higher than normal tissue with a median of 10-15 mmHg. Quantitative autoradiography of frozen tissue slices from rats exposed to ip solutions containing [ $^{14}\text{C}$ ]mannitol or  $^{125}\text{I}$ -immunoglobulin G (IgG; trastuzumab) was performed to determine transport of small and large molecules. With ip pressure = 0-6 mmHg, both mannitol and IgG displayed steep concentration profiles close to the tumor surface with limited penetration deeper within the tumor tissue; antibody penetration was significantly affected by ip pressure. These results demonstrated effects of molecular size, ip pressure, the limited but highly permeable tumor vasculature, and the expanded interstitium on drug penetration from the peritoneal cavity. In conclusion, we have characterized physical and chemical parameters that determine transport of therapeutic agents in our unique tumor-bearing rat model.

**Keywords:** SKOV3, OVCAR3, ovarian carcinoma, diffusion, convection, transport

## INTRODUCTION

Despite complete resection of the primary tumor, metastatic disease from ovarian or colorectal carcinoma often remains on the peritoneum, because the small (5-10 mm dia) tumor nodules cannot be detected by the oncologic surgeon (16;26). Regional (intraperitoneal, ip) therapy for ovarian carcinoma with small molecular weight drugs (MW < 1000 d) has been shown to produce a longer survival time (2). To improve the efficacy of detection and treatment of metastatic tumors, larger molecular weight drugs, including monoclonal antibodies (MAb) which bind to tumor surface antigens, have been used in intraperitoneal therapy (3;22;23;30). Our hypothesis is that since large molecular weight transport is dominated by convection, high ip pressures will increase the delivery of antibody to the tumor. We desired a preclinical model which was adaptable to different types of tumor implantation and which would facilitate the study of physiological and biochemical factors which influence the delivery of chemotherapeutic drugs or immunological agents administered in a large ip volume. Mice are more difficult to maintain under full anesthesia for in vivo studies and are not as easily instrumented as rats for studies which require hours of anesthesia. Therefore we chose to develop a rat model.

The goals of this study include the establishment of a rat model of metastatic intraperitoneal carcinoma for the study of transport of antineoplastic agents and the initial description of physiologic transport properties of the tumor. Most existing rat models have been established by ip injection of tumor cells, which typically results in disseminated implantation on the viscera, in particular, the omentum (24;32). These small visceral tumors are difficult to study mechanistically because the implants are small, and the forces of diffusion and convection are difficult to determine. We report the development of a unique athymic rat model with tumors located in a discreet position in the abdominal wall, which facilitates physiological measurements and surgical manipulations. Human ovarian tumor cell lines were expanded and implanted into the abdominal wall muscle of athymic rats. After sufficient time to produce a palpable tumor nodule, each animal was anesthetized, and one of several protocols was carried out. Included in the physiologic measurements were: intravascular volume measured with two techniques, extracellular volume, tumor permeability, interstitial pressures, penetration profiles of small and large molecules injected ip.

## **METHODS**

### **Animals**

RNU nude rats (150-200 g) were purchased from the National Cancer Institute, Frederick, Maryland. They were housed in the Athymic Animal Facility at the University of Rochester or at a barrier facility at the Laboratory Animal Facility at the University of Mississippi Medical Center. The research protocols had been approved by the local animal Care and Use Committees.

### **Tumor Cells**

Initial batches of the SKOV3 tumor cells were a kind gift from Dr. Joseph Rosenblatt and Dr. Pia Challita-Eid (University of Rochester, Rochester, NY). SKOV3 cell had been shown to overexpress HER2 receptors on their surface and would present a good target for the clinically-relevant monoclonal antibody Trastuzumab (personal communication, Dr. Challita-Eid). Later experiments were performed with SKOV3 or OVCAR3 cells purchased from ATCC, (Rockville, Maryland). The SKOV3 cells were grown at 37° C with the following media: 90% McCoy's 5A medium with 1.5 mM L-glutamine and 2.2g/L sodium bicarbonate (Invitrogen Corp., Carlsbad, CA) supplemented with 10% fetal bovine serum (Sigma, St Louis, MO). The cells multiplied quickly to provide ~10<sup>8</sup> cells in three weeks. NIH:OVCAR-3 cells were grown in modified RPMI-1640 medium from ATCC and supplemented with 10 µg/ml bovine insulin and 20% fetal bovine serum (Sigma). The second tumor cell line was pursued as a possible variant to the SKOV3 tumor in terms of transport characteristics (macroscopic structure, microscopic structure, physiologic variables). The establishment of a second xenograft in athymic rats also confirms the usefulness of the animal model in other applications.

Implantation of other cell lines was attempted but failed to grow in the athymic rats: MDA-MB-231 and MDA-MB-453.

## Isotopic Tracers and Solutions

The solution used as a vehicle to introduce test molecules into the peritoneal cavity or intravenously (iv) was Krebs-Ringer-Bicarbonate (KRB, 290 mosm/kg, pH=7.4) solution (containing as follows (mM): 120 NaCl, 10 KCl, 2 CaCl<sub>2</sub>, 25 NaHCO<sub>3</sub>, 0.28 KH<sub>2</sub>PO<sub>4</sub>, 1.2 MgSO<sub>4</sub>). The solution was filtered with a 0.45- $\mu$ m pore size membrane (Nalgene) and stored at 4°C. Bovine serum albumin (5%) was added to all solutions to be used in the peritoneal cavity; this prevents loss of protein (and oncotic pressure) from the plasma to the fluid in the cavity (9)).

<sup>14</sup>C-mannitol was purchased from Moravek Biochemicals (Brea, Calif) and used directly in experiments designed to measure extravascular space. Isotope detection was performed with a Beckman liquid scintillation counter (LS 6000IC, Beckman Instrument, Inc. or Tricarb 2500-TR, Packard Inst Co, Meridian, Connecticut).

Trastuzumab, the IgG monoclonal antibody to the HER2 receptor, was used as a macromolecular marker, because it was known to bind receptors on SKOV3 cells. It also acts as a general macromolecular marker. It was obtained from the University of Rochester Cancer Center Pharmacy or the University of Mississippi Medical Center Pharmacy and was carefully labeled with <sup>125</sup>I (Amersham Life Science, Arlington, IL) with the Iodo-Beads Iodinating Reagent (Pierce Biochemicals, Rockford, IL). To remove free iodide, the labeled antibody solution was repeatedly diluted, transferred to Centricon-30 tubes (Millipore Corp, Billerica, MA) and centrifuged until the free iodide was less than 1% (see (8) for details). On each experimental day, the <sup>125</sup>I-Trastuzumab was diluted with normal saline and repeatedly centrifuged until free <sup>125</sup>I was less than 1% by precipitation with 10% tricarboxylic acid(8). Gamma counting were measured with Packard Cobra II Auto-Gamma counter or Beckman 8000 gamma counter.

## Surgical Procedures

Tumor Implantation: Animals were allowed to have full access to water and food and acclimatized after arrival in the Athymic Facility for at least one week prior to any surgical manipulations. Tumor cells were harvested on the day of implantation. Implantation was carried

out within 3 hours of harvesting; the viability of post-implantation, harvested cells were tested with trypan blue and demonstrated that more than 85% of the total were viable 4 hours after harvest.

Each animal was anesthetized with 1-5% halothane or isoflurane, 95% oxygen within a laminar airflow hood. Using sterile technique, the skin over the midline of abdominal wall was opened, and a 2 cm vertical incision along the linea alba was made in the abdominal wall muscle to expose the peritoneum. With a syringe and 22 ga needle, cells ( $30-40 \times 10^6$  per site of injection; typical injection volume was 0.2-0.3 ml) were injected into the muscle of the abdominal wall so as to form a sub-peritoneal nodule. As illustrated in Figure 1, the location of implantation was selected because the hydrostatic pressure gradient, used to induce the convection of protein into the tumor, could be easily controlled by manipulating the intraperitoneal pressure. With the ip pressure at zero, pure diffusive transport could be studied. The abdominal wall wound was carefully closed with interrupted simple sutures. The skin was closed with sterile wound clips. The animal was observed to recover and to move around its cage within 15 min following the surgery. Using this procedure, less than 1% of the animals experienced post-operative complications which required termination prior to their use in an experiment.

The tumor cell nodule could be initially palpated through the skin; however, within 24 hours, the nodule would disappear. If the tumor cells formed a solid tumor nodule, it would typically be palpable under the skin within 7-10 days. With both cell lines, approximately 50% of tumor implantations were successful. This success rate was improved to 75% by further immunosuppression of the animal with daily cyclosporine injections (3 mg sc each day); there were no apparent complications from the use of cyclosporine in this dose. Once the tumor had an apparent diameter of greater than 5 mm, it was ready for one of several experimental protocols.

Surgical procedure in preparation for a transport experiment: Because these experiments were typically 4-6 hours in length, the tumor-bearing animals were initially anesthetized with intramuscular sodium pentobarbital (60 mg/kg). After the initial injection and placement of an intravenous (iv) catheter, subsequent injections of anesthetic were made iv. A tracheostomy was performed and catheters were placed intra-arterially to monitor blood pressure (maintained MAP

> 80 mmHg) and to sample blood. An ip catheter was placed through the abdominal wall for instillation and sampling of the ip solution. Temperature was maintained at  $36.5 \pm 1.5$  °C by a warming blanket and heat lamp.

### **Tissue Histopathology and Immunohistochemistry**

All frozen tumor sections were stained with standard Hematoxylin and Eosin and were examined for evidence of necrosis, as evidenced by the lack of nucleated cells or cellular material. Care was taken to insure that all analyses were carried out on non-necrotic tumor.

Immunohistochemistry of CD31, a vascular endothelial cell marker (19), was performed to determine the pattern of angiogenesis in each tumor and to assess total vascular space in the tumor tissue. This stain also permits the comparison of drug penetration profiles into the tumor with the location of the vasculature. Excised tumors were immediately fixed in neutral pH-buffered 4% formalin solution. They were then divided into 3-4 cross sections, embedded in paraffin wax and cut into 4  $\mu$ m sections for CD31 staining. The sections were deparaffinized with xylene and rehydrated with graded alcohols and treated with 0.01M citrate buffer, pH 6.0 for antigen retrieval. Endogenous peroxidase activity was quenched with 3% hydrogen peroxide for 10 min. Staining was performed at room temperature throughout. Non-specific binding sites were blocked with 1.5% donkey serum in phosphate-buffered saline (PBS) for 1 hr. Sections were treated for 30 min with anti-CD31 antibody diluted 1:350 in blocking solution. The slides were washed three times in PBS, treated for 60 min with the biotinylated antibody and washed again. An avidin-biotinylated-horseradish peroxidase complex (30 min incubation) and 3,3'-diaminobenzidine tetrahydrochloride (10 min) were used for detection. The sections were counter stained with Gill's hematoxylin. No significant staining was observed in negative control sections (without primary antibody) run in parallel for each staining. Slides were independently examined by two investigators with a graticule in one eyepiece of microscope at 200x (less dense center area, 0.25 mm<sup>2</sup> grid size) and 400x ("hot areas" with marked increase of vessels in the 0.0625 mm<sup>2</sup> grid) in 5-10 different locations on each tumor. Any CD31 positive cell cluster that was distinguishable from adjacent tumor cells and connective tissue elements was counted as a single vessel.

## Experimental Protocols

Determination of Tumor Vascular Space and Microvascular Permeability: The purpose of these experiments is the determination of the rate of IgG transport from the plasma to the tumor interstitium and the degree of tissue-averaged vascularity. These parameters are important if the animal model is used for iv-delivered therapy or for the drug absorption of ip-delivered small molecular weight drugs. In the experiments in SKOV3-tumor bearing animals, we utilized dual-label quantitative autoradiography to measure the total amount of  $^{125}\text{I}$ -IgG in the tumor 3-4 hours after iv injection and simultaneously to measure the microvascular space within the tumor with a second IgG marker labeled with  $^{131}\text{I}$ , injected 1 min prior to sacrifice of the animal. Samples of plasma are taken every 30 min and counted with a gamma counter to measure the concentration of tracers in the plasma ( $C_{\text{plasma}}(t)$ , cpm/ $\mu\text{l}$ ). After the final plasma samples, the animal was sacrificed by decapitation to rapidly halt blood flow, and the tumor and adjacent normal abdominal wall muscle were quickly frozen in  $-70^\circ\text{C}$  isopentane. The frozen tissue is sliced in a cryomicrotome, and dual-label quantitative autoradiography is carried out as in our previous publication (12) to determine the average concentration of each tracer in the tissue parenchyma ( $C_{\text{tissue}}$ , cpm/mg) at the time of sacrifice ( $t_f$ ). From the  $^{131}\text{I}$ -IgG, the relative vascular space ( $\theta_{IV}$ ,  $\mu\text{l}/\text{mg}$  tissue) is calculated from:

$$\theta_{IV} = \frac{C_{\text{tissue}}^{I131}(t_f)}{C_{\text{plasma}}^{I131}(t_f)} \quad [1]$$

where  $C_{\text{plasma}}^{I131}$  = the plasma concentration (cpm/ $\mu\text{l}$ ) of the second antibody tracer, labeled with  $^{131}\text{I}$  and presumed to occupy the vascular space only, and  $t_f$  = time of euthanasia. In the case of OVCAR3, the tissue-averaged vascular density was determined by QAR and found to be reasonably uniform among different tumors. Therefore, we used separate sets of animals to determine the vascular space and the IgG clearance.

The time-averaged clearance of IgG from the tissue vasculature ( $\bar{R}_{\text{tissue}}$ ,  $\mu\text{l}/\text{mg}/\text{s}$ ) is found from:

$$\bar{R}_{\text{tissue}} = \frac{C_{\text{tissue}}^{I125}(t_f) - C_{\text{plasma}}^{I125}(t_f) \cdot \theta_{IV}}{\int_0^{t_f} C_{\text{plasma}}^{I125}(t) dt} \quad [2]$$

The average plasma loss rate of antibody mass per unit mass of tissue for a given tumor can be estimated from  $\bar{R}_{tissue} \cdot \bar{C}_{plasma}$  /tracer specific activity, where  $\bar{C}_{plasma}$  is equal to the time-averaged plasma concentration. Equation [2] assumes that all tracer leaving the microvasculature remains bound within the tumor or muscle or is located in the tumor interstitium. In our previous study (12), the non-specific binding of the tumor stroma provided a significant trap for IgG; however we cannot rule out some transfer to adjacent normal tissue. The rate of efflux for the tumor will be compared with that of the normal muscle. The vascular space within the tumor and within the normal muscle will be averaged and compared.

Extracellular Space: The purpose of these experiments is to measure the relative extracellular volume in normal tissue and tumor. The relative extracellular space is a major determinant of drug transport through the tissue, and it is important to quantify when studying drug diffusion and convection through the tumor. To do this, a bolus of  $^{14}\text{C}$ -mannitol is injected iv into an anesthetized, tumor-bearing rat. The tracer is then continuously infused at a rate to maintain the plasma concentration at a constant value. The plasma is sampled every 15 min for one hour to verify the concentration. At the end of the hour, the animal is sacrificed by decapitation in order to rapidly halt blood flow, and the tissue is rapidly frozen. The tissue is sliced and processed for quantitative autoradiography to determine the tracer concentration in the tissue at the time of sacrifice ( $C_{tissue}(t_f)$ , cpm/mg). The plasma samples are counted to determine the tracer concentration ( $C_{plasma}$ , cpm/ $\mu\text{l}$ ). The extracellular volume relative to the tissue weight ( $\theta_{ECV}$ ,  $\mu\text{l}/\text{mg}$  tissue) is calculated as follows:

$$\theta_{ECV} = \frac{C_{tissue}(t_f)}{\bar{C}_{plasma}} \quad [3]$$

where  $\bar{C}_{plasma}$  is the time-averaged tracer concentration in the plasma. To determine an estimate of the relative interstitial volume ( $\theta_{ISV}$ ,  $\mu\text{l}/\text{mg}$  tissue):

$$\theta_{ISV} = \theta_{ECV} - \theta_{IV} \quad [4]$$

Penetration Studies: The purpose of this procedure was to assess whether intraperitoneal pressures of 0 to 8 mmHg influenced the penetration of ip-administered macromolecules (IgG)

into the tissue surrounding the cavity and to compare the macromolecular transport with that of a small molecule (mannitol).

Just prior to the experiment, 50-100  $\mu\text{Ci}$  of  $^{125}\text{I}$ -Herceptin was mixed in 100 ml of the Krebs solution, containing 5% BSA and 0.5% Evans Blue dye (to mark the contact area and penetration of tissue); this was warmed to 37-39°C. In experiments with  $^{14}\text{C}$ -mannitol, 25  $\mu\text{Ci}$  were mixed with 100 ml of the Krebs solution, containing 5% BSA.

To begin a low-pressure (LP) study, the cavity was opened and a small plastic chamber was affixed to the peritoneal side of the tumor with cyanoacrylate glue and filled with 2-3 ml of fluid. We have used these chambers for transport studies of the normal peritoneum and have shown that the transport across the tissue within the chamber is unaffected by the presence of the chamber (11). The height of this fluid was maintained at < 1 cm in order to insure a low hydrostatic pressure. The chamber insured fluid contact with the tumor and minimal pressure. Samples were collected hourly and at the end of 3 hours, the fluid was removed and, after euthanasia, the tumor was rapidly frozen. It was subsequently processed for autoradiography.

To initiate a high-pressure (HP) penetration study, sufficient solution of the warm solution was injected ip to raise the pressure to 3 mm Hg, and the remainder of the solution was placed in a reservoir connected to the ip catheter via tubing. The reservoir was raised to a level above the right heart to exert 4-8 mmHg of hydrostatic pressure in the cavity. The ip pressure rose to the desired pressure over 15 min and then became steady thereafter; the pressure was verified by glass manometer connected through a three-way valve to the ip catheter. Occasionally, an animal developed respiratory distress and the pressure (volume) in the cavity had to be reduced by ~1 mmHg. Blood and peritoneal fluid were sampled each hour for 1-3 hours. Vital signs were carefully monitored throughout the experiment. Tissue pressure measurements were attempted throughout the experiment. At the end of the experiment, the animal was given an overdose of sodium pentobarbital, and the cavity was opened by laparotomy and the fluid was removed. The animal was then frozen rapidly with isopentane cooled in dry ice (-70°C). The exposed tumor and adjacent normal tissue were cut from the frozen carcass and maintained at -70°C until processed for autoradiography.

## **Analytical Techniques**

Measurement of interstitial pressure: The hydrostatic pressure profile within normal abdominal wall and within tumor tissue was measured with the technique of Wiig and colleagues (34) and Boucher and colleagues (4), as later modified by Flessner(10;14). The technique employs a micropipette mounted on a precision micromanipulator, which is used to penetrate the tissue in precise increments of 100-200  $\mu\text{m}$  from the subcutaneous side inward toward the cavity. The micropipette is connected via a hydraulic system to a servo-null micropressure system (IPM 5A, Institute for Physiology and Medicine, Los Angeles) to determine the actual pressure in mm Hg. Details of the procedure are found in our previous publication (14). The stroma of the tumors was difficult to penetrate 3-4 mm with the glass pipettes, which often broke prior to completing the measurement; this limited the number of pressure profiles to one to three which were obtained in any one tumor. In some cases, the “wick-in-needle” technique (WIN) was used as documented in Fadnes (7), Boucher (5) and Wiig (34) to verify the mean pressure at 1-3 mm depth.

Quantitative Autoradiography (QAR): Sections (10-20  $\mu\text{m}$ ) were cut from frozen specimens with a Hacker-Bright Cryomicrotome and were heat-dried to prevent further transport of the labeled Trastuzumab. The sections were placed with standards (tissues with known isotope concentration) against X-ray film (Kodak Biomax MR) to produce autoradiograms. After development, the films were analyzed with a computerized densitometer (MCID, Imaging Research Inc, St Catherines, Ontario, Canada), which measures optical density versus position in the tissue. The isotopic standards are used to construct a calibration curve (concentration vs OD) to convert the unknown ODs from the tissue samples to concentration. After exposure to film, the tissue slides were stained with hematoxylin and eosin. The device has the capability to superimpose the histologic image and the autoradiographic image; the concentration profile is then measured by superimposing a computational grid over the tissue as illustrated in Figure 2. The average OD within each box of the grid or the average OD within a larger area are determined and automatically converted to concentration. By carefully superposition, the concentration vs position curve or mean concentration of a large area was obtained (see (12)).

In the case of two isotopes, a blocking layer of plastic was placed between the film and the radioactive tissue. This allowed the separation of the high-energy isotope ( $^{131}\text{I}$ ) from the lower energy one ( $^{125}\text{I}$ ). After the high-energy autoradiogram was developed, the tissues were stored for 10 half-lives of the high-energy isotope and then reapplied to the film to obtain the autoradiograms of the lower energy isotope. Each film was then analyzed as in the paragraph above.

### **Calculations and Statistics**

Calculations were performed with Microsoft Excel (v 97 or 2000). Statistical calculations were performed with NCCS (Provo, Utah). Data are presented as mean  $\pm$  SE. Tissue concentrations were typically normalized by dividing by the concentration in the peritoneal cavity or by the plasma concentration in accordance with formulae given above. Quantities were judged to be significantly different if the probability of a Type I error was  $\leq 0.05$  ( $p \leq 0.05$ ).

## **RESULTS**

### **Tumor Implantation: Observations of Metastases**

The tumor cell nodule size could be estimated by palpating the tumor through the skin and approximating the limits of the raised tissue. However, the tumors often developed in various shapes with irregular penetrations through the boundaries of the normal abdominal wall muscle, including the interior boundary, the peritoneum. The true size of the tumor was often not apparent until the peritoneal cavity had been opened. Some of the SKOV3 implantations were allowed to grow beyond four weeks and were observed to produce small white nodules or plaques on the liver, spleen, omentum, and the peri-aortic lymph nodes. This form of metastasis is consistent with the spread of ovarian cancer. None of the OVCAR3 tumors were observed to form metastases, but their growth period was limited to 4 weeks.

## **Tumor Physiologic Properties (summarized in Table 1)**

### SKOV3 tumors

The relative vascular space determined by QAR was averaged over 5-10 sections of each of five different tumors and was found to be ( $\mu\text{l}/\text{mg}$  tissue, mean  $\pm$  SE):  $0.0087 \pm 0.0030$ , while it was  $0.0094 \pm 0.0021$  in normal abdominal wall muscle (NS,  $p > .5$ ). Because QAR is performed on the entire tumor and therefore averages the results for all regions of the tumor, a second method of estimation was used. Figure 3a demonstrates a typical anti-CD-31 stain of an SKOV3 tumor. Since the CD-31 receptor marks all endothelial cells in the tissue, perfused as well as non-perfused vessels will be stained. The staining is concentrated around the edge of the tumor, with very little staining in the center of the nodule. The vessel density of the “hot” (increased vascular density) areas of the tumor averaged (mean  $\pm$  SE,  $n = 10$ , vessels/ $\text{mm}^2$ ):  $617 \pm 66$ . In the less dense, center areas of the tumors, the vessel density averaged:  $23.7 \pm 1.6$  vessels/ $\text{mm}^2$ .

In order to compare the CD-31 measurements with the QAR results, an assumption of the vessel cross-sectional area must be made and then multiplied by the number of vessels and the relative contribution of the “hot areas” to the total tumor. If each vessel is assumed to have an average radius of 6-12  $\mu\text{m}$  or  $6 \times 10^{-3}$  to  $12 \times 10^{-3}$  mm (19), the areas for each vessel range from 0.000113 to 0.000452  $\text{mm}^2$  ( $\pi \bullet \text{radius}^2$ ). From the product of vessel density times the area of a single microvessel, the area-density of the vessels in the hot areas is calculated to be  $0.070 \pm 0.01$  to  $0.28 \pm 0.04$   $\text{mm}^2/\text{mm}^2$ , while that of the less dense areas is  $0.003 \pm 0.000$  to  $0.012 \pm 0.001$   $\text{mm}^2/\text{mm}^2$ . Because the hot area is approximately 8.5% of the total area of tumor, the overall average for the entire tumor cross section equals 0.009 to 0.036 ( $(.085 \times 0.07 + .915 \times 0.003) = 0.0087$ ). The value for the QAR measurement, which reflects the tissue-averaged concentration of perfused vessels rather than total number of vessels, falls within this range.

The relative extracellular space was found to be ( $n = 5$ ,  $\mu\text{l}/\text{mg}$  tissue, mean  $\pm$  SE):  $0.54 \pm 0.11$  for the tumor, while it was  $0.22 \pm 0.06$  in the adjacent normal muscle of the abdominal wall. These would correspond to approximate interstitial spaces (= extracellular space – vascular space) of 0.53 and 0.21 in tumor and muscle, respectively.

Vascular permeability to IgG was estimated by measuring the total deposition in tissue versus time and subtracting that portion of the antibody which was contained within the vasculature (see Eqn [2]). The average clearance was estimated to be (n=6,  $\mu\text{l/hr/mg}$  tissue, mean  $\pm$  SE):  $0.00885 \pm 0.00057$ , while that of adjacent muscle (n=6) was  $0.00477 \pm 0.00223$  (NS at  $p < .05$ ).

### OVCAR3 Tumors

The relative vascular space determined by QAR was averaged over 5-10 sections of each of five different tumors and was found to be ( $\mu\text{l/mg}$  tissue, mean  $\pm$  SE):  $0.0109 \pm 0.0010$  and was not significantly different than previous measurements in muscle ( $p > 0.5$ ). As in the case of the SKOV3 tumor, a second method of estimation was used. Figure 3b demonstrates a typical anti-CD-31 stain of an OVCAR3 tumor. The staining is concentrated around multiple, distinct nodules within the tumor, which present a distinctly different pattern from the SKOV3 tumors. The vessel density of the hot areas of the tumor averaged (mean  $\pm$  SE, n = 17, vessels/ $\text{mm}^2$ ):  $225 \pm 10$ . In the less dense, center areas of the tumor nodules, the vessel density averaged:  $15.5 \pm 2.1$  vessels/ $\text{mm}^2$ . If we make the same assumptions and calculations as with the SKOV3 results, the area-density of the vessels in the hot areas is  $0.026 \pm 0.011$  to  $0.102 \pm 0.046$   $\text{mm}^2/\text{mm}^2$ , while that of the less dense areas is  $0.0018 \pm 0.0002$  to  $0.007 \pm 0.001$   $\text{mm}^2/\text{mm}^2$ . Because the hot area is 22% of the total, the overall average equals  $0.007 - .028$  ( $(.22 \times 0.026 + .78 \times 0.0018) = .0071$ ). As with the SKOV3 tumors, the QAR results falls within the calculated range of areas resulting from the CD-31 determinations.

The relative extracellular space was found to be (n = 6,  $\mu\text{l/mg}$  tissue, mean  $\pm$  SE):  $0.61 \pm 0.03$  for the tumor, which is significantly different from the adjacent normal muscle of the abdominal wall ( $0.22 \pm 0.06$ ). The tumor interstitial spaces (= extracellular space – vascular space) would be approximately 0.60.

Vascular permeability was found to be (n=5,  $\mu\text{l/hr/mg}$  tissue, mean  $\pm$  SE):  $0.0147 \pm 0.0024$ , while that of adjacent muscle (n=6) was  $0.00595 \pm 0.00219$  (Sig,  $p < .05$ ).

## **Tumor Interstitial Pressures**

Figures 4a and 4b illustrate the peak and mean pressures for SKOV3 and OVCAR3 tumors, as determined with the micropipette-servo null system. The peak pressure is defined as the highest pressure recorded as the glass pipette is advanced 3-4 mm through the tumor; the mean pressure is the average of all readings within the tumor parenchyma. The range of pressure for both tumors was 0 to 32 mmHg, while the median pressures were 10-15 mm Hg. The tumor pressures are quite variable within individual tumors and between xenografts from the same cell line. Peak pressures sometimes occurred at 300-400  $\mu\text{m}$  from the surface, but typically were higher at 1500-2000  $\mu\text{m}$ . The typical size of these tumors was on the order of 3-10 mm in diameter, with some oval or cylindrical in shape and others with more spherical shape. As shown in the figures, peak pressures and mean pressures do not appear to correlate with tumor size; however, most of the tumors sampled were relatively small because of the design of the study.

## **Tumor Penetration of Mab: Low vs High IP Pressure**

### Small molecules: [ $^{14}\text{C}$ ]mannitol

The average concentration profile of mannitol ( $n=5$ ,  $\text{mean}\pm\text{SE}$ ) after 60 min (tissue concentration profiles for small solutes approach a pseudo-steady state after 30 min (13)) is illustrated in Figure 5. In these experiments, the cavity was filled with a large volume of isotonic solution containing [ $^{14}\text{C}$ ]mannitol, and the ip pressure was maintained at 4-6 mmHg for the duration of the experiment. These demonstrate that the drug at the tumor edge has concentration of 0.22 relative to the final concentration in the peritoneal cavity. The profile then decreases to a low steady-state value of  $\sim 8\%$  of the concentration in the cavity within 800  $\mu\text{m}$  of the surface. The flat profile beyond 800  $\mu\text{m}$  in the tumor corresponds to the center portion of the tumor nodules, which have a very low density of blood vessels (see Figure 4a).

Six animals with SKOV3 implants were fitted with small chambers over the peritoneal side of the tumor. The solution height was kept  $< 1$  cm to minimize pressure and to set up a transport situation of nearly pure diffusion. The profiles at 180 min in Figure 5 demonstrate little penetration with very low tumor levels of labeled IgG. Tissue concentration profiles in SKOV3

tumor-bearing animals after 180 min at an ip hydrostatic pressure of 6-8 mmHg are also shown in Figure 5 for comparison and demonstrate a significant effect of higher intraperitoneal pressure which aids in the penetration of the antibody. This observation supports our hypothesis that increased ip pressure will deliver more antibody into the tumor.

## **DISCUSSION**

### **Animal Model**

We have successfully implanted SKOV-3 and OVCAR-3 human ovarian tumor cells into the abdominal wall muscle of athymic rats. This has permitted us to simulate a metastatic tumor nodule in the parietal peritoneum and to control the chemical and physical forces of transport for drugs administered in the peritoneal cavity. The novel tumor location permits the measurement and manipulation of forces and the determination of the transport outcome. If sufficient time is allowed for tumor growth, further metastasis occurs in the peritoneal cavity. In our prior rat model of ip carcinoma (12), we used a human melanoma cell line (FEMX-II) to create an analogous model, but the FEMX-II did not metastasize from the primary site of implantation. Other models in rats differ from ours because of the goal to create ascites (1) or bulky pelvic tumors (20;28) which do not readily permit manipulation of pressure forces necessary for ip-injected macromolecules.

Other models of intraperitoneal cancer have been created in mice. Ozols et al (28) treated a murine ovarian tumor with Adriamycin; administration of equivalent doses of the drug demonstrated nearly two orders of magnitude higher tumor drug levels after ip injection versus iv, which supports the later findings of efficacy in humans (2). Ong and Mattes (27) set up an ascitic ovarian model in nude mice and studied routes of treatment with monoclonal antibodies to cell surface receptors; they did not study specific maneuvers to improve ip delivery. Wahl and colleagues (33) studied distribution of ip injected antibodies in tumor bearing mice and showed that during the first 48 hours of treatment, there was a significant therapeutic advantage compared to iv injection. Ito and colleagues (21) implanted LS174T human colon cancer in the peritoneal cavities of mice; when they compared IgG tumor profiles after iv injection with those

from a small volume-ip injection of IgG, they observed a less uniform IgG concentration profile but higher concentrations in the tumor periphery. The major differences between these studies and our study are the positioning of the tumor and the use of the athymic rat as the tumor host which permits specific physiologic maneuvers and measurements which are difficult in mice.

## **In Vivo Physiologic Measurements of Tumor**

### Tumor vascular space

The location and density of the tumor vascular space is important in understanding of drug transport within the tumor. The lack of uniformity leads to perturbations of how rapidly the concentration is dissipated within the parenchyma of the target. This is illustrated by a comparison of the  $^{14}\text{C}$ -mannitol profile in Figure 5 with the vascular pattern in Figure 3a. The lack of blood vessels results in a marked decrease in the removal rate of mannitol from the central portion of the tumor. On the other hand, the variation in vasculature has little effect on the transport of macromolecules, since they are removed from tissue by lymphatics, which are typically not functional in tumors (29).

The tumor vascular space in each tumor implant was estimated by quantitative autoradiography to be approximately 0.009-0.01 ml/g tumor one min after injection of a labeled protein. This was essentially the same as that of the adjacent normal tissue, and these values are similar to our previous measurement of 0.01 ml/g abdominal wall muscle of a different rat species (36). The fact that the tissue-averaged, relative tumor vascular space is the same as that of normal muscle is a serendipitous finding, since tumor vasculature is highly variable, as illustrated by Figures 3a and 3b.

There are few comparable measurements of the tumor vascular space. In chambers mounted on the back of mice, relatively thin, transparent tumors have been grown for study (25). However, capillary densities were measured as microvascular length divided by the area of observation. Unfortunately, the numbers are not easily transformed into volume/g tissue units. In a subsequent study of this tumor, the vascular volume averaged  $0.092 \pm 0.029$  (vol vessels/vol

tumor) (35). In an earlier study which employed intravascular tracers, Gullino and Grantham (17) found that the vascular space varied from 1% for a fibrosarcoma to 12.4% for Hepatoma HC. Thus, the SKOV-3 and OVCAR-3 tumors are at the lower end of range of vascular volumes within tumors.

To verify the relatively low fraction of tissue which is occupied by blood vessels, we have performed immunohistochemistry to detect the relative number of potential vessels in the tumor tissue. We discovered two distinctive patterns in the two tumor types. OVCAR-3 appeared to form smaller nodules with areas of high density of staining in the connective tissue surrounding each small tumor nodule. SKOV3, on the other hand, formed larger nodules which, if left to grow beyond 8-10 mm in diameter, became necrotic in the center. The areas of increased angiogenesis were chiefly in the periphery of the tumor or tumor nodule. The CD-31 staining does not permit differentiation between perfused and non-perfused vessels. However, by assuming a range of average vessel diameters and calculating the potential contribution of each region to the overall vascular density, there appears to be good agreement between the CD-31 staining and the tissue-averaged values from QAR.

#### Tumor extracellular space

The transport of a water-soluble substance through tissue is directly proportional to the degree of “porosity” or extracellular space in the tissue (8). Under the condition of no fluid in the peritoneal cavity, the extracellular spaces in the SKOV-3 and OVCAR-3 tumors were  $0.54 \pm 0.11$  and  $0.61 \pm 0.03$  ml/g tissue, respectively. With the assumption of a vascular volume of approximately 0.01 ml/g tissue, these would translate into approximate values for the interstitial space of 53 and 60 ml/100 g tissue, respectively. The interstitial space of normal abdominal wall muscle in Sprague-Dawley rats was previously determined to be 16 ml/100 g of tissue (36), comparable to that found in the muscle of athymics,  $0.22 \pm 0.06$ . Early work by Gullino and colleagues (18) demonstrated similar values for normal muscle in rats, while tumor interstitial spaces varied from 50-74 ml/100 g for hepatomas to nearly 80% for fibrosarcoma transplanted into rodents. This large interstitial space is thought to result from the lack of lymphatics and the high interstitial pressure (25-30 mmHg in Walker 256 carcinoma) (15). Thus the finding of an interstitial space in tumors which is 2.5 times that of normal tissue is consistent with the

measurements by other groups. The expanded interstitium should promote penetration of the drug into the tumor.

### Tumor vascular permeability

The whole-tumor technique which we used to determine the clearance of the antibody from the tumor provides a tissue-averaged value and is limited in that it does not provide measurements of the intrinsic permeability of the capillaries. Taking into account that the areas which contain the vasculature make up 10-20% of the tumor nodule, the true permeability of the vessels in these areas is likely 5-10 times the value derived from the whole tissue QAR. Gerlowski and Jain (15) demonstrated the VX2 carcinoma growing in a rabbit ear chamber had a permeability to dextran 150 (nominal MW of 150,000 daltons) of  $57.2 \times 10^{-8}$  cm/s, while granulation tissue was  $7.3 \times 10^{-8}$  (ratio of ~8). These values are not easily transposed to whole-tissue values, which we have calculated. Yuan and colleagues (35) studied the permeability of adenocarcinoma LS174T using the dorsal chamber in SCID mice. They found the PS/V (ml/min/cc tissue) for labeled albumin to be  $7.56 \times 10^{-3}$  in the tumor, which is appropriately larger than the permeability of the SKOV-3 to the larger IgG molecule used in our study. That these tumors had limited vascular space and were slightly leakier than normal vessels favors the efficacy of regional delivery rather than system iv delivery.

### Tumor interstitial pressures

Figure 4 displays the interstitial pressures of both types of tumors. The high tumor pressures in SKOV-3 and OVCAR3 tumors are similar to measurements in human melanoma (6) and in cervical cancer (31). These pressures differ from the normal pressure of the abdominal wall muscle, which is slightly negative (34;36). These high pressures present a significant challenge to the delivery of antibodies from the periphery of the tumor or from the circulation (5).

### **Penetration of antibody into SKOV-3 tumors**

Figures 5 clearly demonstrates the effect of pressure on the transport of an IgG antibody into SKOV-3 tumors. However, the relatively high interstitial pressures of Figures 4a and 4b are likely a major factor in the lower concentration within tumor when compared to normal tissue

(14). The mannitol, which transports chiefly via diffusion, demonstrates rapid dissipation in the tumor periphery due to the presence of highly permeable blood vessels, but the concentration of agent delivered is significantly higher than the macromolecule. If the high pressure could be maintained in the cavity for long periods of time, the IgG tumor concentration profiles would be expected to increase in magnitude with a greater duration of the experiment due to binding and the relative lack of functional lymphatics in the tumor (29). Further studies on the characteristics of the interaction between the Trastuzumab molecule and SKOV3 tumor cells will be required to elucidate these mechanisms.

### **Acknowledgment**

This work was supported through a grant from the National Cancer Institute: RO1 CA085984. Angela Williams, Joanne Lofthouse at the University of Rochester, Rochester, New York and Lori Genous at the University of Mississippi provided superb technical assistance.

## List of Figures

1. Design of experimental model. Tumor cells are implanted in the abdominal wall and allowed to grow into a nodule which protrudes into the peritoneal cavity. This position facilitates examination of growth of the tumor, the control of pressure forces across the tumor, and pressure measurements within the tumor during the experiment.
2. Autoradiographic image of a section of anterior abdominal wall containing three tumor nodules in an athymic rat. The optical density varies with the concentration of  $^{125}\text{I}$ -IgG, which has transported in via a solution placed in the peritoneal cavity at an ip pressure of 4-6 mmHg. The computational grid demonstrates how the MCID software averages the OD for each small rectangle; this is converted to an average concentration. The concentration versus distance is then tabulated. The lack of penetration of IgG (darkness in the film) is evident in the autoradiogram.
3. CD-31 staining in tumors (magnification = 240x). **A.** Edge of SKOV3 tumor nodule showing staining of vessels which are in the tissue surrounding the tumor nodule. Little staining is in the center of the nodule. **B.** OVCAR-3 nodule which displays CD-31 staining in the periphery of a tumor nodule. Despite the small size of these tumor nodules, there is little staining in its center.
4. **A.** Peak (closed circles) and mean pressures (open circles) in each of 15 OVCAR3 tumors versus tumor volume. **B.** Peak (closed circles) and mean (open circles) pressures in each of 12 SKOV3 tumors versus tumor volume.
5. Penetration of [ $^{14}\text{C}$ ]mannitol after 60 min and  $^{125}\text{I}$ -IgG after 180 min (mean  $\pm$  SE concentration normalized to the average peritoneal fluid concentration,  $C_{\text{PF}}$ ) into SKOV3 tumors from solution at low pressure (< 1 mmHg) and at high pressure (6-8 mmHg). Open symbols refer to the low pressure experiments (n=6), while solid symbols refer to higher pressure experiments (n=18). This figure demonstrates very low IgG concentrations with low pressure forces in the cavity. Higher pressures result in higher IgG concentrations in the tumor. The transport of the smaller molecular weight mannitol is diffusion-dominated, and its penetration is blunted by rapid absorption in the tumor periphery. The concentration profile levels off in the central region of the tumor nodules where there are few vessels.

## Reference List

1. Agostino A, Robin F, Jais JP, Aggerbeck M, Vilde F, Blanc B, Lecuru F: Peritoneal closure reduces port site metastases: results of an experiment in a rat ovarian cancer model. *Surgical Endoscopy* 2002; 16:289-291
2. Alberts DS, Liu PY, Hannigan EV, O'Toole R, Williams SD, Young JA, Franklin EW, Clarke-Pearson DL, Malviya VK, DuBeshter B: Intraperitoneal cisplatin plus intravenous cyclophosphamide versus intravenous cisplatin plus intravenous cyclophosphamide for stage III ovarian cancer. *New Engl J Med* 1996; 335:1950-1955
3. Alvarez RD, Partridge EE, Khazaeli MB, Plott G, Austin M, Kilgore L, Russell CD, Liu T, Grizzle WE, Schlom J, LoBuglio AF, Meredith RF: Intraperitoneal radioimmunotherapy of ovarian cancer with <sup>177</sup>Lu-CC49: a phase I/II study. *Gyn Oncol* 1997; 65:94-101
4. Boucher Y, Baxter LT, Jain RK: Interstitial pressure gradients in tissue-isolated and subcutaneous tumors: implications for therapy. *Cancer Res.* 1990; 50:4478-4484
5. Boucher Y, Jain R.K.: Microvascular pressure is the principal driving force for interstitial hypertension in solid tumors: implications for vascular collapse. *Cancer Res* 1992; 52:5110-5114

6. Boucher Y, Kirkwood JM, Opacic D, Desantis M, Jain RK: Interstitial hypertension in superficial metastatic melanomas in humans. *Cancer Res* 1991; 51:6691-6694
7. Fadnes HO, Reed RK, Aukland K: Interstitial fluid pressure in rats measured with a modified wick technique. *Microvasc.Res.* 1985; 29:176-189
8. Flessner M.F., Lofthouse J., Zakaria ER: In vivo diffusion of immunoglobulin G in muscle: effects of binding, solute exclusion, and lymphatic removal. *Am.J.Physiol.* 1997; 273:H2783-H2793
9. Flessner MF: *Transport of Water-Soluble Solutes Between the Peritoneal Cavity and Plasma in the Rat* Ann Arbor, MI, Univ. of Michigan, 1981
10. Flessner MF: Osmotic barrier of the parietal peritoneum. *Am.J.Physiol.* 1994; 267:F861-F870
11. Flessner MF: Small-solute transport across specific peritoneal tissue surfaces in the rat. *J.Am.Soc.Nephrol.* 1996; 7:225-233
12. Flessner MF, Dedrick RL: Monoclonal antibody delivery to intraperitoneal tumors in rats: effects of route of administration and intraperitoneal solution osmolality. *Cancer Res.* 1994; 54:4376-4384

13. Flessner MF, Dedrick RL, Schultz JS: A distributed model of peritoneal-plasma transport: theoretical considerations. *Am.J.Physiol.* 1984; 246:R597-R607
14. Flessner MF, Schwab A: Pressure threshold for fluid loss from the peritoneal cavity. *Am.J.Physiol.* 1996; 270:F377-F390
15. Gerlowski LE, Jain RK: Microvascular permeability of normal and neoplastic tissues. *Microvasc.Res.* 1986; 31:288-305
16. Gershenson DM, Tortolero-Luna G, Malpica A, Baker VV, Whitaker L, Johnson E, Mitchell MF: Ovarian intraepithelial neoplasia and ovarian cancer. *Obstetrics and Gynecol Clinics of North America* 1996; 23:475-543
17. Gullino PM, Grantham FH: The vascular space of growing tumors. *Cancer Res* 1964; 24:1727-1732
18. Gullino PM, Grantham FH, Smith SH: The interstitial water space of tumors. *Cancer Res* 1965; 25:727-731
19. Hasan J, Byers R, Jayson GC: Intra-tumoral microvessel density in human solid tumors. *Brit J Cancer* 2002; 86:1566-1577

20. Hornung R, Fehr MK, Monti-Frayne J, Krasieva TB, Tromberg BJ, Berns MW, Tadir Y: Highly selective targeting of ovarian cancer with the photosensitizer PEG-m-THPC in a rat model. *Photochemistry and Photobiology* 1999; 70:624-629

21. Ito T, Griffin TW, Collins JA, Brill AB: Intratumoral and whole-body distributions of C110 anti-carcinoembryonic antigen radioimmunotoxin (RIT) after intraperitoneal and intravenous injection: a quantitative autoradiographic study. *Cancer Res.* 1992; 52:1961-1967

22. Kairemo KJ: Radioimmunotherapy of solid cancer: a review. *Acta Oncol* 1996; 35:343-355

23. Kievit E, Pinedo HM, Schluper HM, Boven E: Addition of cisplatin improves efficiency of I-131-labelled monoclonal antibody 323/A3 in experimental human ovarian cancer. *Intl J Radiol Oncology, Biology, Physics* 2004; 38:419-428

24. Lecuru F, Guilbaud N, Agostini A, Augereau C, Vilde F, Taurelle R: Description of two new ovarian carcinoma models in nude rats suitable for laparoscopic experimentation. *Surgical Endoscopy* 2001; 15:1346-1352

25. Leunig M, Yuan F, Menger MD, Boucher Y, Goetz AE, Messmer K, Jain RK: Angiogenesis, microvascular architecture, microhemodynamics, and interstitial fluid pressure during early growth of human adenocarcinoma LS174T in SCID mice. *Cancer Res* 1992; 52:6553-6560

26. Markman M: Intraperitoneal therapy of ovarian carcinoma. *Semin Oncol* 1998; 25:356-360
27. Ong GL, Mattes MJ: Penetration and binding of antibodies in experimental human solid tumors grown in mice. *Cancer Res.* 1989; 49:4264-4273
28. Ozols RF, Locker GY, Doroshow JH: Pharmacokinetics of adriamycin and tissue penetration in murine ovarian cancer. *Cancer Res.* 1979; 39:3209-3214
29. Padera TP, Kadambi A, diTomaso E, Carrelra CM, Brown EB, Boucher Y, Chol NC, Mithisen D, Wain J, Mark EJ, Munn LL, Jain RK: Lymphatic metastasis in the absence of functional intratumor lymphatics. *Science* 2002; 296:1883-1887
30. Quadri SM, Malik AB, Tang XZ, Patenia R, Freedman RS, Briesendorp HM: Preclinical analysis of intraperitoneal administration of In-111-labeled human tumor reactive monoclonal IgM AC6C3-2B12. *Cancer Res* 1995; 55 (23 Suppl):5736s-5742s
31. Roh HD, Boucher Y, Kalnicki S, Buchsbaum R, Bloomer WD, Jain R.K.: Interstitial hypertension in carcinoma of uterine cervix in patients: possible correlation with tumor oxygenation and radiation exposure. *Cancer Res* 1991; 51:6695-6698
32. Rose GS, Tocco LM, Granger GA, DiSaia PJ, Hamilton TC, Santin AD, Hiserodt JC: Development and characterization of a clinically useful animal model of epithelial ovarian cancer in the Fischer 344 rat. *Am J Obstet Gynecol* 1996; 175:593-599

33. Wahl RL, Barrett J, Geatti O, Liebert M, Wilson BS, Fisher S, Wagner JG: The intraperitoneal delivery of radiolabeled monoclonal antibodies: studies on the regional delivery advantage. *Cancer Immunol Immunother* 1988; 26:187-201
  
34. Wiig H, Reed RK, Aukland K: Micropuncture measurement of interstitial fluid pressure in rat subcutis and skeletal muscle: comparison to the wick-in-needle technique. *Microvasc.Res.* 1981; 21:308-319
  
35. Yuan F, Leunig M, Berk DA, Jain RK: Microvascular permeability of albumin, vascular surface area, and vascular volume measured in human adenocarcinoma LS174T using dorsal chamber in SCID mice. *Microvasc.Res.* 1993; 45:269-289
  
36. Zakaria ER, Lofthouse J, Flessner MF: In vivo effects of hydrostatic pressure on interstitium of abdominal wall muscle. *Am.J.Physiol.* 1999; 276:H517-H529

**Table 1: Anatomic and Physiologic Characteristics of Tumors**

<b>Parameter</b>	<b>Units</b>	<b>Normal Muscle</b>	<b>SKOV3 Tumor</b>	<b>OVCAR3 Tumor</b>
<b>CD-31 Staining High Density Area</b>	Vessels/mm <sup>2</sup> mean±SE	not measured	617±66 n = 10	225±10 n = 17
<b>CD-31 Staining Low Density Area</b>	Vessels/mm <sup>2</sup> mean±SE	not measured	23.7±1.6 n = 10	15.5±2.1 n = 17
<b>Relative vascular space*</b>	μl/mg tissue mean±SE	0.0094±0.0021 n = 5	0.0087±0.0030 n = 5 NS	0.0109±0.0010 n = 5 NS
<b>Relative Extracellular Space*</b>	μl/mg tissue mean±SE	0.22±0.06 n = 5	0.54±0.11 n = 5 p<.05	0.61±0.03 n = 6 p<.05
<b>IgG Clearance*</b>	μl/hr/mg tissue mean±SE	0.00477±0.00223 0.00595±0.00219 n = 6, each	0.00885±0.00057 n = 6 NS	0.0147±0.0024 n = 5 p<.05

\*Comparison of tumor characteristics with normal muscle were evaluated for p < 0.05.

## Experimental Design

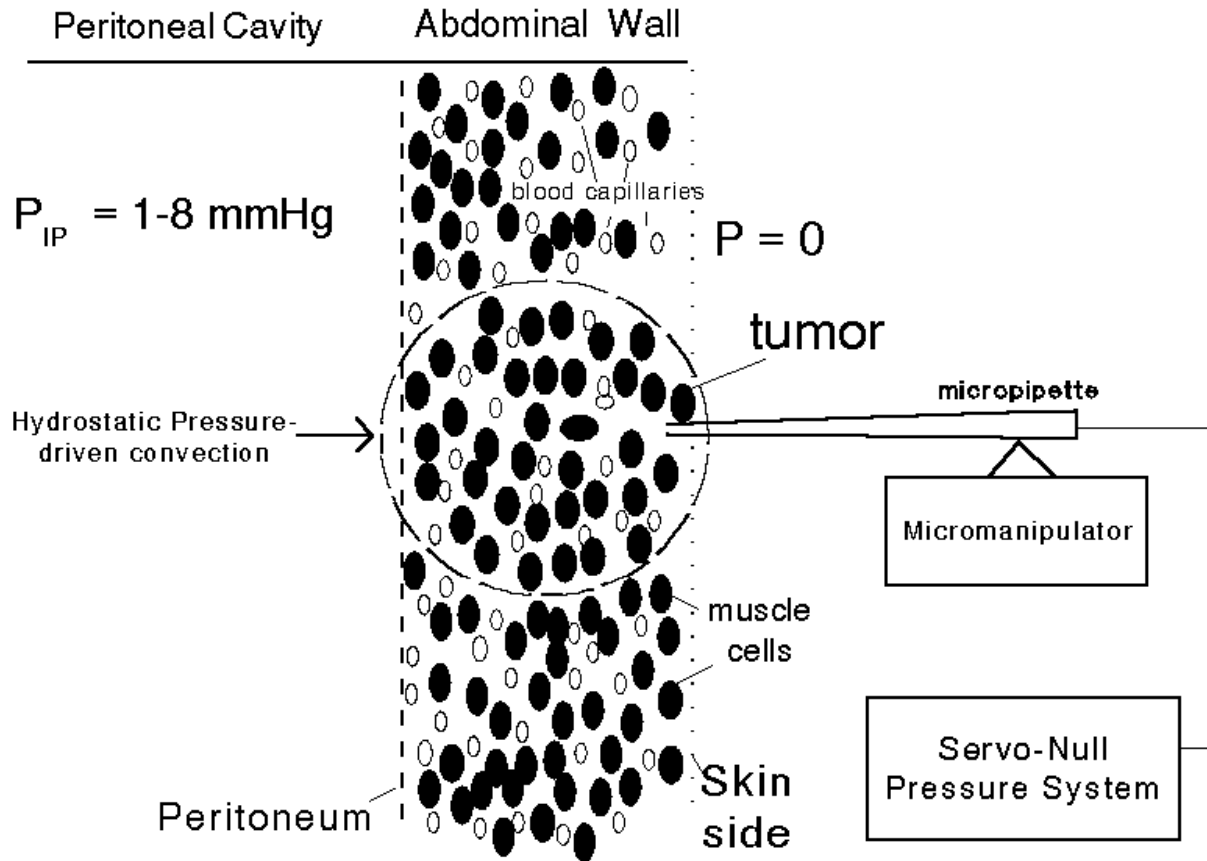


**Figure 1:** Design of experimental model. Tumor cells are implanted in the abdominal wall and allowed to grow into a nodule which protrudes into the peritoneal cavity. This position facilitates examination of growth of the tumor, the control of pressure forces across the tumor, and pressure measurements within the tumor during the experiment.

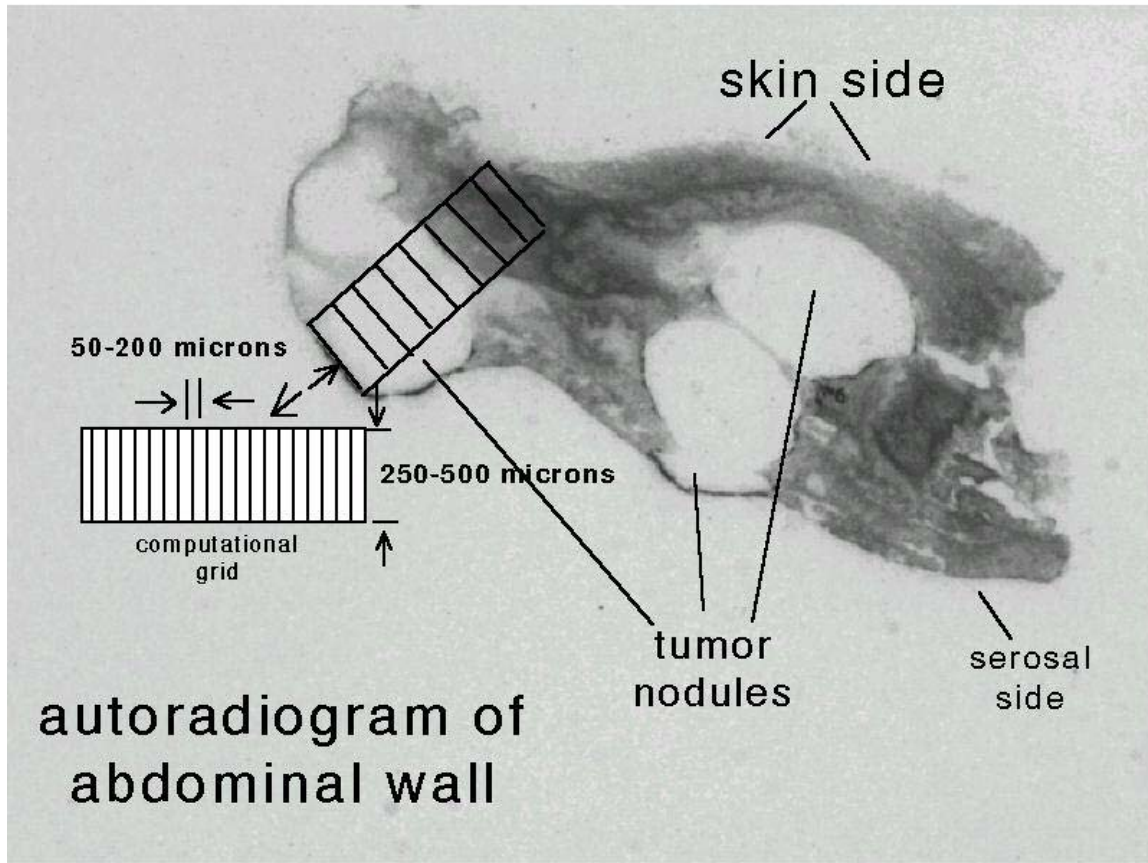
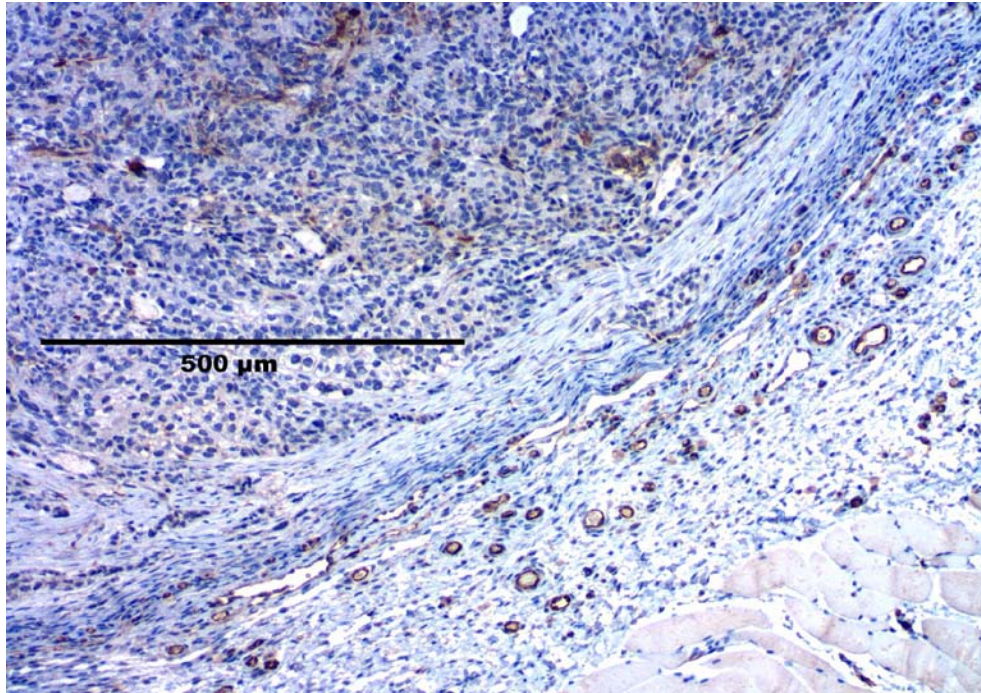
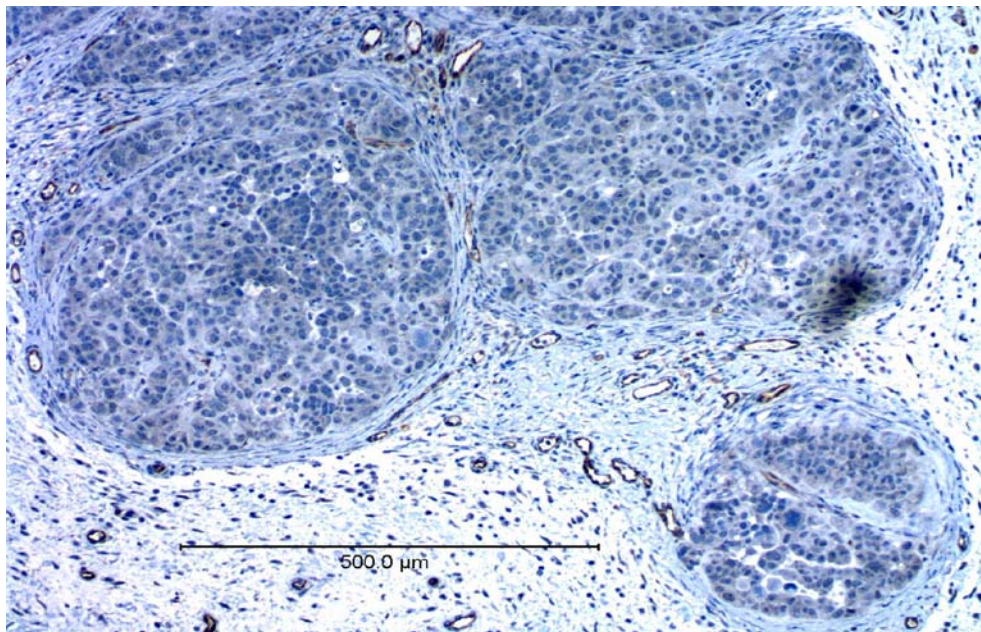


**Figure 2:** Autoradiographic image of a section of anterior abdominal wall containing three tumor nodules in an athymic rat. The optical density varies with the concentration of  $^{125}\text{I}$ -IgG, which has transported in via a solution placed in the peritoneal cavity at an i.p. pressure of 4-6 mmHg. The computational grid demonstrates how the MCID software averages the OD for each small rectangle; this is converted to an average concentration. The concentration versus distance is then tabulated. The lack of penetration of IgG (darkness in the film) is evident in the autoradiogram.

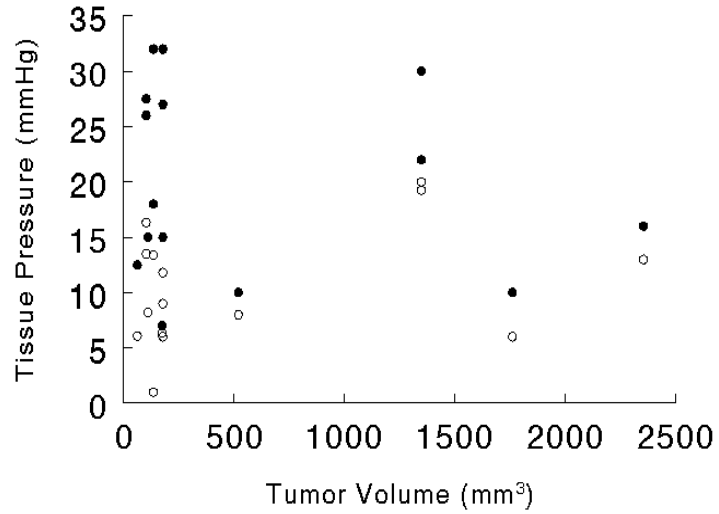


**A**

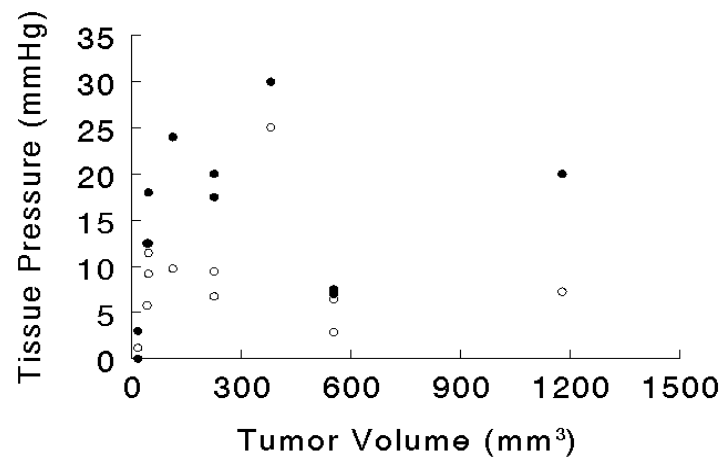


**B**

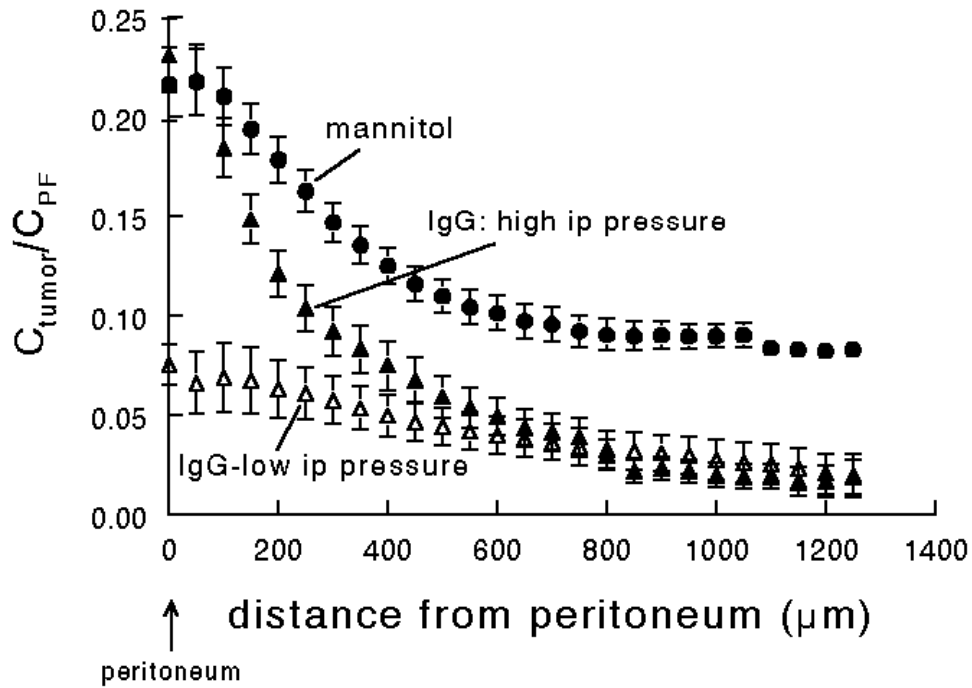
**3** CD-31 staining in tumors (magnification = 100x). **A.** Edge of SKOV3 tumor nodule showing staining of vessels which are in the tissue surrounding the tumor nodule. Variable staining is in the center of the nodule. **B.** OVCAR-3 nodule which displays CD-31 staining in the periphery of tumor nodules. Despite the small size of these tumor nodules, there is little staining in their centers.



**Figure 4A** Peak (closed circles) and mean pressures (open circles) in each of 15 OVCAR3 tumors versus tumor volume.



**Figure 4B** Peak (closed circles) and mean (open circles) pressures in each of 12 SKOV3 tumors versus tumor volume.



6. **Figure 5:** Penetration of [<sup>14</sup>C]mannitol after 60 min and <sup>125</sup>I-IgG after 180 min (mean ± SE concentration normalized to the average peritoneal fluid concentration, C<sub>PF</sub>) into SKOV3 tumors from solution at low pressure (< 1 mmHg) and at high pressure (6-8 mmHg). Open symbols refer to the low pressure experiments (n=6), while solid symbols refer to higher pressure experiments (n=18). This figure demonstrates very low IgG concentrations with low pressure forces in the cavity. Higher pressures result in higher IgG concentrations in the tumor. The transport of the smaller molecular weight mannitol is diffusion-dominated, and its penetration is blunted by rapid absorption in the tumor periphery. The concentration profile levels off in the central region of the tumor nodules where there are few vessels.